Journal of The Electrochemical Society, **163** (8) G99-G106 (2016)
0013-4651/2016/163(8)/G99/8/$33.00 © The Electrochemical Society

Methylviologen Mediated Electrosynthesis of Palladium Nanoparticles Stabilized with CTAC

Gulnaz R. Nasretdinova,[a] Yuri N. Osin,[b] Aidar T. Gubaidullin,[a] and Vitaliy V. Yanilkin[a,z]

[a]*A. E. Arbuzov Institute of Organic and Physical Chemistry, Kazan Scientific Center, Russian Academy of Sciences, 420088 Kazan, Russia*
[b]*Kazan Federal University, Interdisciplinary Center for Analytical Microscopy, 420018 Kazan, Russia*

Efficient electrosynthesis of ultrasmall palladium nanoparticles stabilized with CTA^+ cetyltrimethylammonium cations ($Pd@CTA^+$) was carried out in an aqueous medium by methylviologen mediated electroreduction of poorly soluble aggregates $([PdCl_4]^{2-} \cdot 2CTA^+)_n$ of $[PdCl_4]^{2-}$ anionic complex with CTA^+ cations on a glassy carbon electrode at potentials of the $MV^{2+}/MV^{\bullet+}$ redox couple. $([PdCl_4]^{2-} \cdot 2CTA^+)_n$ aggregates are reduced directly on the electrode at a low rate and the generated metal is deposited on the electrode. In the case of mediated reduction, the metal is not deposited on the cathode, and after passing of Q = 2 F quantitative conversion from $[PdCl_4]^{2-}$ to $Pd@CTA^+$ nanoparticles occurs in the solution bulk. These particles are positively charged (zeta-potential is 66.8 mV) and their hydrodynamic diameter is 18 nm. Separated Pd@CTAC nanoparticles are combined into larger aggregates due to coalescence of the organic shell. The predominant shape of metal nanoparticles is an imperfect sphere with a diameter of 5 ± 3 nm, and the average size of the metal crystallites is 4.66 nm.

Manuscript submitted April 19, 2016; revised manuscript received May 24, 2016. Published June 4, 2016.

In recent years, metal nanoparticles (MNP) have been attracting increasing interest due to their unique properties and due to the wide variety of their practical uses in catalysis, electronics, biomedicine, optics, analysis, etc.[1–7] The most developed and popular method for their preparation involves chemical reduction of metal ions and complexes in solution using a variety of reducing agents. Electrochemistry is quite widely used for MNP preparation on an electrode surface,[8] but it is rarely used for production of metal particle dispersions (sols). This is primarily due to the fact that when metal ions and complexes are reduced on an electrode, the generated metal is usually deposited on the latter. In the presence of MNP stabilizers, the proportion of the deposited metal decreases but still remains quite high. For example, in the preparation of silver NP by reduction of silver ions in the presence of polyvinylpyrrolidone that is widely used for MNP stabilization, the proportion of deposited metal is 80%.[8,9] Therefore, in all the methods developed for MNP electrosynthesis in solution bulk, the deposition problem is solved in some way. In the pulse sonoelectrochemistry method,[10–12] this problem is solved by combining the process of MNP generation on an electrode surface during electroreduction for a short time with its subsequent transfer into the solution by sonication of the working electrode. In the method by Reetz et al.,[13–23] electroreduction of ions is carried out in aprotic organic media using salts of surfactant cations, such as tetraalkylammonium or phosphonium, as a supporting electrolyte. For these purposes we have proposed a method of mediated electrosynthesis[24–34] which differs from the above-mentioned electrochemical methods in such a way that the step of metal ion reduction is moved from the electrode surface into the solution bulk. In this case, a mediator is reduced on the cathode and the reduced form of the mediator diffuses into solution bulk where it reduces the metal ion or complex. Thus, deposition of the metal on the electrode is completely prevented or minimized. The feasibility of the method and its efficiency have been recently demonstrated by the examples of preparation of Pd,[24–28] Ag,[29–32] Co,[33] Au[34] NP in the absence and presence of stabilizers in aqueous, aqueous-organic and non-aqueous media from metal salts and complexes, or from metal ions generated in situ in solution upon dissolution of a metal anode during electrolysis. The method is equally efficient with soluble ions and complexes ($[PdCl_4]^{2-}$, Ag^+, AuCl, $[CoCl_4]^{2-}$) and insoluble metal salts (AgCl, spherical AgCl@CTAC NP), irrespective of whether reduction of the mediator on the electrode is easier or harder than reduction of the of metal substrate.

PdNP are of undoubted interest, especially as catalysts in various reactions, particularly hydrogen evolution,[35,36] carbon–carbon cross-coupling reactions such as Suzuki,[37–43] Heck,[44,45] Sonogashiro[46] and Stille coupling.[47,48] The catalytic properties depend on the size, shape of the metal crystal and nature of the stabilizing shell.[7,35,36] The general trend is that the smaller the size of NP, the higher its catalytic activity.[7] Therefore, the problem reduces to obtaining the ultrasmall NP (<10 nm) of a certain size and shape. This type of particles are mainly obtained by chemical reduction of ions and complexes of Pd(II) by different reducing agents.

Ultrasmall spherical PdNP were also successfully obtained by methylviologen mediated electrosynthesis at potentials of the $MV^{2+}/MV^{\bullet+}$ redox couple.[24–28] In aqueous medium in the presence of silica nanoparticles modified by alkylamino groups, PdNP are stabilized in the surface layer of silica particles.[27] The synthesis of these particles also occurs efficiently if tetraviologen calix[4] resorcines are used in monomeric form[24–26] or in the form of porous spherical copolymer NP[28] as a mediator and simultaneously as an MNP stabilizer. In the latter case, PdNP are encapsulated in the pores of the polymer particles. In development of the mediated electrosynthesis method, in this study we investigated methylviologen mediated electrosynthesis of ultrasmall PdNP in an aqueous medium in the presence of cetyltrimethylammonium chloride (CTAC), a typical representative of salts of surfactant cations widely used as stabilizers.

Experimental

The study was performed using cyclic voltammetry (CV), dynamic light scattering (DLS), preparative electrolysis, scanning electron microscopy (SEM), scanning transmission electron microscopy (STEM), high resolution transmission electron microscopy (HRTEM), X-ray powder diffraction (XRPD) and UV-visible spectroscopy techniques.

Chemicals.—Methylviologen dichloride $MV^{2+} \cdot 2Cl^-$ (Acros Organics), $PdCl_2$ (Aldrich), cetyltrimethylammonium chloride CTAC (Acros Oraganics), and NaCl were used as purchased without additional purification. Twice distilled water was used as the solvent.

Cyclic voltammograms (CV curves) were recorded in argon atmosphere at various potential scan rates using a P-30S potentiostat (without IR-compensation). A glassy carbon (GC) disk electrode (3.4 mm diameter) pressed into Teflon was used as the working electrode. The electrode was cleaned by mechanical polishing before each measurement. Platinum wire was used as the counter electrode. The potentials were measured relative to aqueous saturated calomel electrode (SCE), E_0' $(Fc/Fc^+) = +0.41$ V. The aqueous SCE was connected by a bridge filled with the supporting solution. The temperature was 295 K.

Preparative electrolysis was carried out in a three-electrode cell separated with a porous glass diaphragm in potentiostatic mode (−0.9 V vs. SCE), in argon atmosphere at room temperature

[z]E-mail: yanilkin@iopc.ru

(T = 295 K) using a P-30S potentiostat. During the electrolysis, the solution (H_20, 0.02 M CTAC, 2 mM $MV^{2+}{\cdot}2Cl^-$, 1.5 mM $PdCl_2$, V = 20 ml) was stirred with a magnetic stirrer. A GC plate (S = 4.5 cm^2) was used as the working electrode. An SCE connected by a bridge filled with the supporting solution was used as the reference electrode. A Pt wire immersed in the supporting solution was used as the auxiliary electrode. When the electrolysis was over, the solution was studied by CV on an indicator GC disk electrode (3.4 mm diameter) directly in the electrolysis cell, as well as by DLS.

For SEM, STEM, HRTEM, DLS and XRPD measurements, the Pd@CTAC NP formed in the electrolysis were separated by centrifugation (15,000 rpm), first time for 2.5 hours and then 3 times for half-hour periods, each time with elutriation of the solution above the precipitate. The solution above the precipitate was colored dark brown. The separation of the solution from the precipitate was not complete, so a small amount of the solution remained. This suspension was examined by XRPD. For SEM, STEM, HRTEM and DLS, the suspension was dispersed in double-distilled water by sonication. In the case of SEM, the resulting solution was applied to the surface of a titanium foil previously purified by sonication in water and acetone. Then the sample was exsiccated in air by low heating (not higher than 40°C). In STEM and HRTEM analyses, 10 microliters of the sample suspension was deposited on a formvar (tm)/carbon coated 3 mm copper grid, which was then dried at room temperature. After complete drying, the grid was placed into a transmission electron microscope in a special graphite holder for microanalysis.

The hydrodynamic diameter and zeta potential of the particles in solution were measured by DLS. The measurements were performed using Malvern Instrument Zetasizer Nano. The measured autocorrelation functions were analyzed with Malvern DTS software.

Electron microscopic analysis.—The morphology of the sample surfaces was characterized in plan-view with SEM using a high resolution Merlin microscope from Carl Zeiss combined with ASB (Angle Selective Backscattering), SE InLens (Secondary Electrons Energy selective Backscattering) and STEM detectors, which was also equipped for energy-dispersive X-ray spectroscopy (EDX) analysis with AZTEC X-MAX energy-dispersion spectrometer from Oxford Instruments. HRTEM analysis of NP was carried out using a Hitachi HT7700 Excellence transmission scanning electron microscope. The examination was performed at accelerating voltages of 80 kV–100 kV in TEM mode.

XRPD studies of the samples were performed on a Bruker D8 Advance automatic X-ray diffractometer equipped with a Vario attachment and a Vantec linear coordinate detector. Cu $K_{\alpha 1}$ (λ 1.54063 Å) radiation monochromated by a curved Johansson monochromator was used. The operating mode of the X-ray tube was 40 kV, 40 mA. Room-temperature data were collected in the Bragg-Brentano geometry with a flat-plate sample.

A sample in liquid form was applied on a silicon plate that decreased background scattering. After drying of the layer, a few more layers were applied over it to increase the total amount of the sample. Patterns were recorded in the 2Θ range between 3° and 90°, in 0.008° steps, with a step time of 0.1–5.0 s. Several diffraction patterns in various experimental modes and with different step times were collected for the sample.

Processing of the data obtained was performed using EVA.[49] X-ray powder diffraction database PDF-2 (ICDD PDF-2, Release 2005–2009) was used to identify the crystalline phase. Full-profile analysis of diffraction data by the Rietveld method with minimization of the discrepancy between the experimental and theoretical curves was made using TOPAS V.3.1 software package.[50] The results of the refinement are as follows: R_{exp} = 2.34%, R_{wp} = 4.45%, R_p = 2.73%, GOF = 1.90. Based on the refinement results, the dimensional characteristics of the palladium crystallites were calculated.

UV-visible spectra were recorded on a Perkin-Elmer Lambda 25 spectrometer.

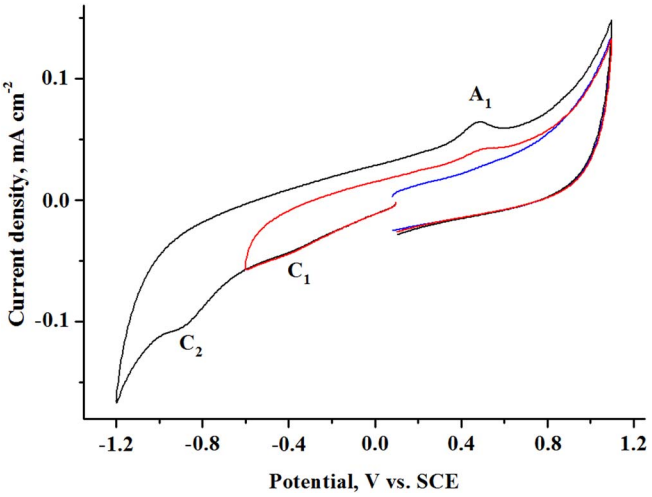

Figure 1. CV curves of $[PdCl_4]^{2-}$ (1.5 mM) in water /0.02 M CTAC medium. $E_{start.}$ = 0.10 V. ν = 100 mV/s.

Results and Discussion

Cyclic voltammetry.—The $PdCl_2$ salt is poorly soluble in water/0.02 M CTAC medium. At the calculated concentration of 1.5 mM, $PdCl_2$ can be dissolved only by sonication combined with magnetic stirring and heating to ~60°C. This gives a pink-yellow transparent solution that becomes turbid at room temperature. A light precipitate appears on prolonged keeping without stirring. The CV curve of this system contains no peaks in the available region of anodic potentials (to +1.10 V vs. SCE). In the cathodic region, the C_2 peak is recorded at E_{C2} = −0.92 V (Figure 1) and a faint peak C_1 is observed at less cathodic potentials ($E_{C1} \approx -0.40$ B). When potential is reversed after both reduction peaks, A_1 reoxidation peak of metallic palladium Pd^0[24–28] deposited on the electrode appears at E_{A1} = 0.48 V on the return anodic branch of the CV curve (Figure 1).

Keeping the electrode at the potential of the first reduction peak (E = −0.50 V) leads to accumulation of metallic palladium on the electrode. Its amount increases with exposure time (Figure 2a). Under these conditions, the C_1 peak on the return cathodic branch is shifted toward less cathodic potentials ($E_{C1'}$ = −0.06 V) and increases with exposure time, whereas the C_2 peak remains unchanged.

Exposure of the working electrode at the potential of the second reduction peak (E = −0.90 V) leads to the same effects as exposure at the potential of the first peak, i.e., accumulation of about the same amount of metallic palladium on the electrode depending on the electrolysis time (peak A_1, Figure 2b), the same shift of C_1 toward less cathodic potentials, and the same growth of this peak. The only difference is that an additional A_2 peak appears at $E_{A2} \sim -0.20$ V and its height increases with the time of electrolysis.

In water /0.02 M NaCl medium, i.e. upon replacement of CTAC for NaCl, and within a similar procedure $PdCl_2$ dissolves rather easily to form a transparent yellow solution; the solution remains homogeneous after cooling to room temperature. The CV curve recorded in this solution, as well as in the CTAC supporting solution, contains no peaks in the anodic region. Two reduction peaks are recorded in the cathodic region but at much less cathodic potentials (E_{C1} = −0.06 and E_{C2} = −0.28 V, Figure 3). The intensity of the first predominant peak is significantly higher than that in the supporting CTAC solution, and the height of the second peak is of the same order. If the potential is reversed after the first reduction peak, a rise of the oxidation current of deposited metallic Pd^0 is observed at ~ 0.30 V on the return anodic branch of the CV curve (Figure 3). If potential is reversed after the second reduction peak, the A_2 peak of reoxidation of adsorbed hydrogen (atomic or molecular)[24] appears additionally at E_{A2} = −0.21 V. It is evident that the second reduction peak corresponds to

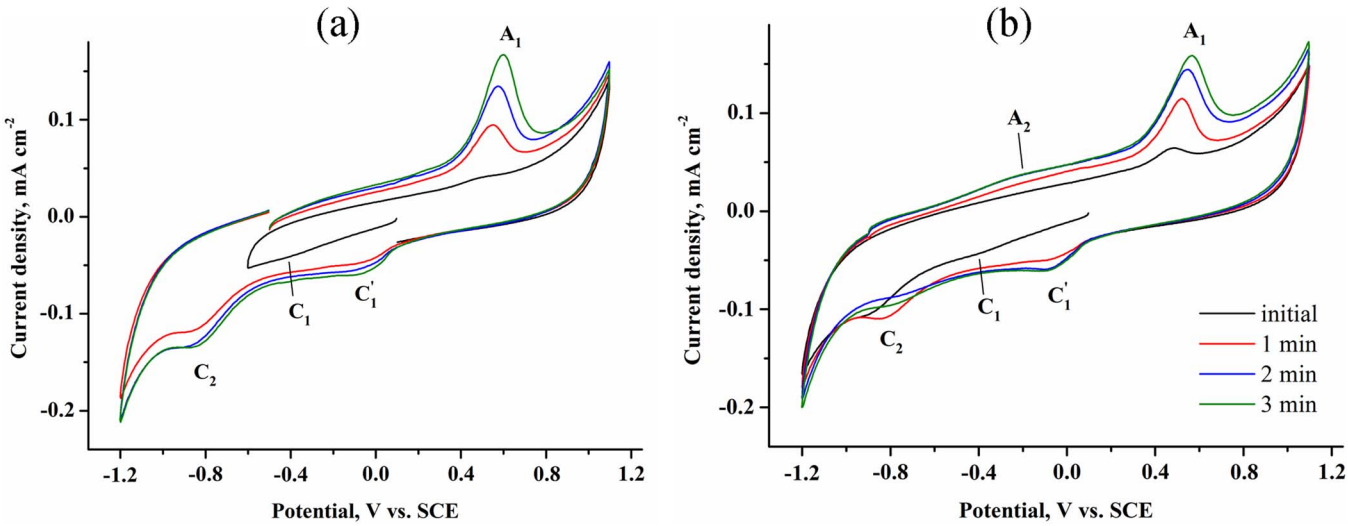

Figure 2. CV curves of $[PdCl_4]^{2-}$ (1.5 mM) in water /0.02 M CTAC medium after keeping the electrode at (a) E = −0.50 V (b) E = −0.90 V for various periods. ν = 100 mV/s.

electrocatalytic hydrogen evolution on metallic palladium deposited on the GC electrode.

The results obtained in supporting NaCl solution allow us to interpret the voltammetric data in supporting CTAC solution. In the presence of excess amount of Cl^-, $PdCl_2$ forms the $[PdCl_4]^{2-}$ complex dianion[51] which is bound with CTA^+ and precipitates over time. The C_1' peak corresponds to $[PdCl_4]^{2-}$ reduction and apparently C_1 corresponds to the reduction of $([PdCl_4]^{2-} \cdot 2CTA^+)_n$ aggregates. It follows from the small value of the C_1 peak current in the initial solution (Figure 1) that the major fraction of the complex dianion is present in the precipitate. The presence of the C_1' peak and the absence of the C_1 peak after oxidation of electrogenerated metallic palladium particles (Figure 2) show the slowness of formation of aggregates from $[PdCl_4]^{2-}$ and CTA^+ on the time scale of CV recording (seconds). The second C_2 peak, like in supporting NaCl solution, is due to electrocatalytic reduction of medium components to form hydrogen. However, in supporting CTAC solution this process is apparently hindered by adsorption of CTA^+ cations on the deposited metal surface.

The CV curve of the $[PdCl_4]^{2-}$ (1.5 mM) – MV^{2+} (2 mM) mixture shows three reduction peaks and two reoxidation peaks (E_{C3} = −0.80 V, $E_{C3'}$ = −1.00 V, E_{C4} = −1.15 V, E_{A3} = −0.55 V, E_{A4} = −0.87 V) typical of MV^{2+} in supporting CTAC solution[32] (Figure 4). The cathodic peaks are due to reduction of methylviologen, both free (C_3) and bounded in CTAC micelles (C_3') to the radical cation $MV^{\bullet+}$ and subsequent reduction of $MV^{\bullet+}$ to neutral diamine MV^0 (C_4). The anodic peaks correspond to the oxidation of free radical cation $MV^{\bullet+}$ (A_3) and diamine (A_4). The presence of $[PdCl_4]^{2-}$ in the system is indicated only by low-intensity C_1 and A_1 peaks.

Keeping the working electrode at the potential of the C_1 peak (E = −0.5 V) leads to appearance of the A_1 peak of oxidation of metallic Pd^0 deposited on the electrode, and a more or less pronounced $[PdCl_4]^{2-}$ reduction peak appears on the reverse cathodic branch at $E_{C1'}$ = −0.15 V (Figure 5a). These peaks increase with an increase in the exposure time. These data indicate that the presence of MV^{2+} in solution does not affect the electrochemical behavior of $[PdCl_4]^{2-}$. However, deposition of metallic palladium on the GC electrode affects the CV curves of MV^{2+}. There are no peaks of reduction of MV^{2+} bound with CTAC (C_3'); only two reversible MV^{2+} reduction peaks (peaks C_3 and C_4, Figure 5b) are recorded, like in supporting NaCl solution without CTAC.[32] If the generated metal is oxidized beforehand, the C_3' peak with a lower intensity than in the starting solution is recorded (Figure 5a). The importance of the role of deposited palladium in the electrochemical behavior of methylviologen is evident,

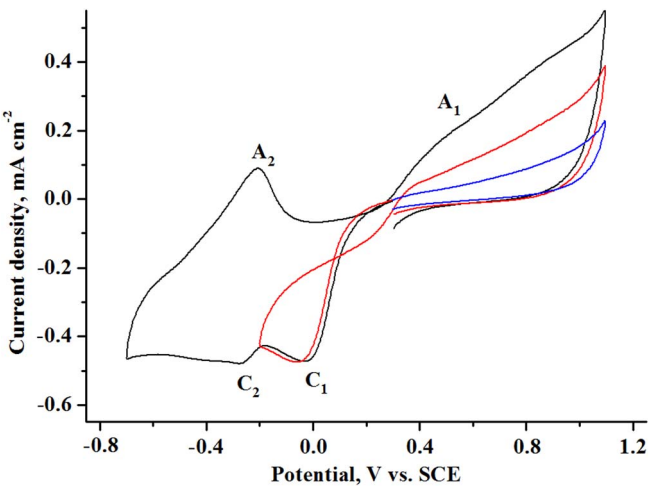

Figure 3. CV curves of $[PdCl_4]^{2-}$ (1.5 mM) in water /0.02 M NaCl medium. $E_{start.}$ = 0.30 V. ν = 100 mV/s.

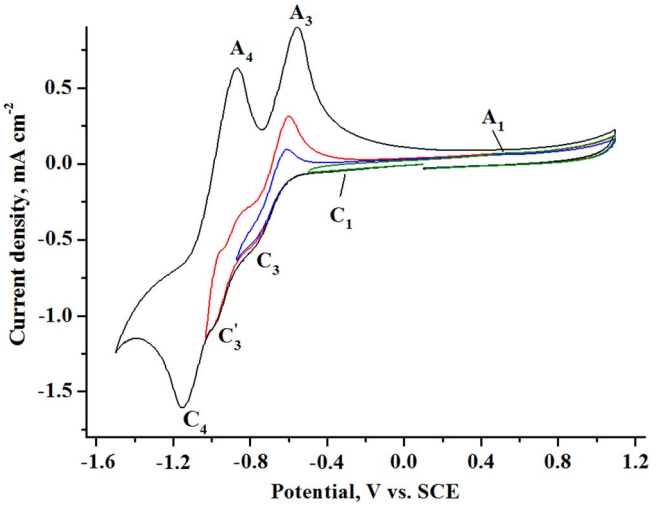

Figure 4. CV curves of the $[PdCl_4]^{2-}$ (1.5 mM) – MV^{2+} (2 mM) system in water /0.02 M CTAC medium. $E_{start.}$ = 0.10 B. ν = 100 mV/s.

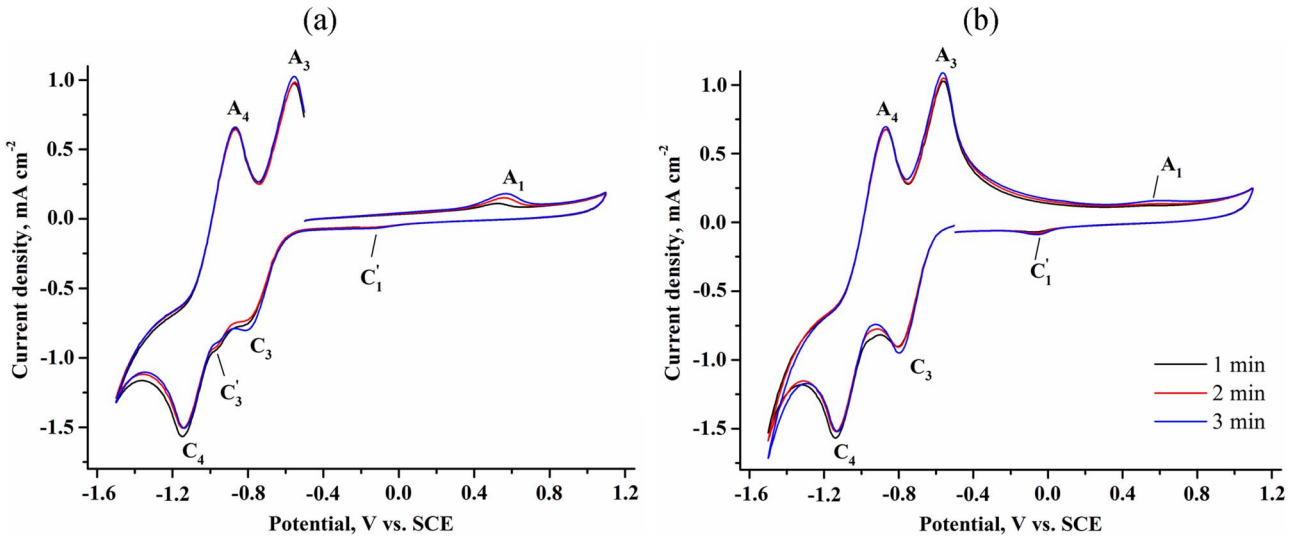

Figure 5. CV curves of the $[PdCl_4]^{2-}$ (1.5 mM) – MV^{2+} (2 mM) system in water /0.02 M CTAC medium after keeping the electrode at E = −0.50 V for various periods with the potential scan in (a) negative and (b) positive directions. ν = 100 mV/s.

but the reasons of such a strong influence are not so obvious. CTAC is certainly bound on the surface of deposited metallic palladium, but it is unlikely to occur quantitatively, because CTAC is used in large excess. Perhaps, other micelles of methylviologen with CTAC are formed in the presence of metallic palladium, and the reduction of methylviologen, both free and bound in micelles, at the same potential becomes possible. When Pd^0 is oxidized, slow restructuring of these micelles into the initial micelles occurs. So during the time of CV curves are recorded, the initial micelles are not formed quantitatively and the C_3' peak of lower intensity is recorded on the CV curve (Figure 5a).

It follows from the CV curves (Figure 6) recorded after exposure of the electrode at the potential of the $MV^{2+}/MV^{\bullet+}$ redox couple (E = −0.90 V) that the height of the A_3 reoxidation peak of the radical cation did not change with an increase in the exposure time. Therefore, $MV^{\bullet+}$ is not adsorbed on the electrode surface. The A_1 peak of Pd^0 reoxidation is almost absent on the anodic branch of the curve, thus the process of mediated reduction of $([PdCl_4]^{2-} \cdot 2CTA^+)_n$ aggregates (Scheme 1) runs efficiently and they are not reduced on the electrode.

Preparative electrolysis.—Preparative electrolysis was carried out in a solution with the same composition as that used for CV. The reduction was performed in a diaphragm cell at the controlled potential of reduction of the mediator to a radical cation (E = −0.90 V). The solution gradually darkened during the electrolysis, and its turbidity gradually disappeared. By the end of the electrolysis, after passing Q = 2F with respect to $[PdCl_4]^{2-}$ (54 min), the solution was dark brown (see Figure 7). Nothing precipitated on the working electrode (its weight did not change during the electrolysis) and on the walls and bottom of the cell.

After electrolysis, the CV curve of the system changed insignificantly (Figure 8a). The C_1 peak of $[PdCl_4]^{2-}$ reduction disappeared in the cathodic region, the total number of peaks and the total height of the MV^{2+} reduction peaks did not change, but the ratio of the C_3 and C_3' peak heights changed in favor of the latter.

There is no peak of metallic palladium oxidation in the anodic region. However, if the electrode is previously kept in the electrolysis cell without applying the potential and without stirring, a small peak (A_1) appears at E = 0.57 V (Figure 8b).

The UV-visible spectrum of the solution of the separated particles shows only the absorption peak of a residual amount of MV^{2+} at 256 nm.

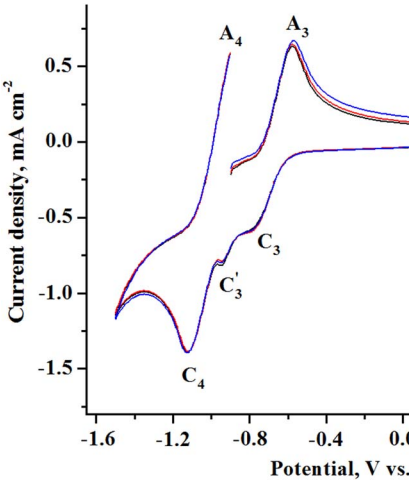

Figure 6. CV curves of the $[PdCl_4]^{2-}$ (1.5 mM) – MV^{2+} (2 mM) system in water /0.02 M CTAC medium after keeping the electrode at E = −0.90 V for various periods. ν = 100 mV/s.

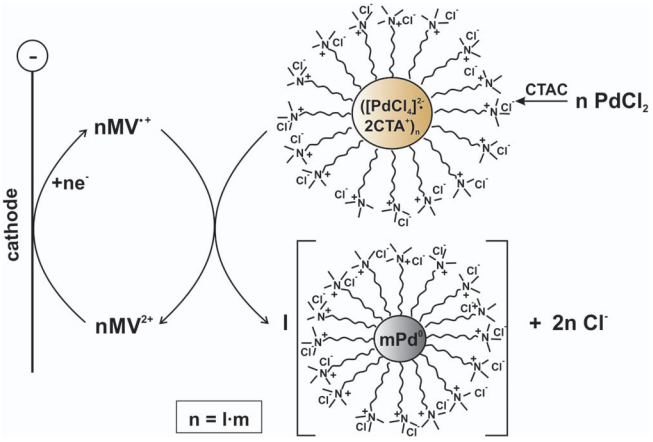

Scheme 1. Methylviologen mediated electrosynthesis of Pd@CTAC nanoparticles.

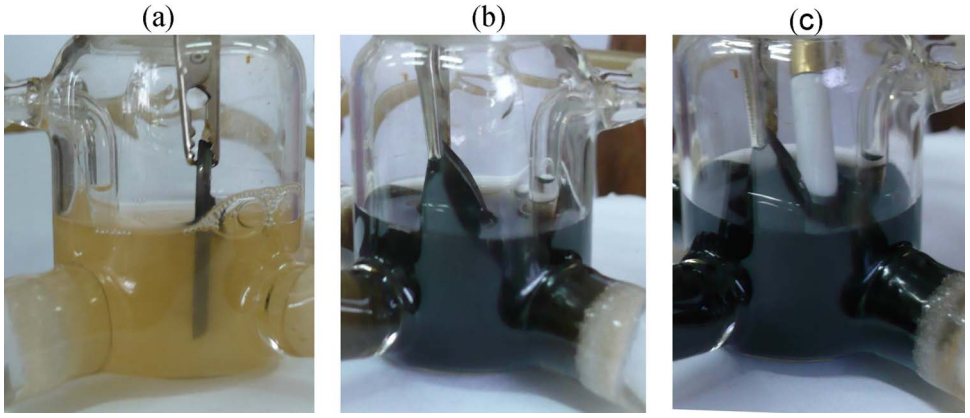

Figure 7. Change in the solution color during preparative methylviologen-mediated electroreduction of $[PdCl_4]^{2-}$ in aqueous media depending on the quantity of electricity Q with respect to $[PdCl_4]^{2-}$: (a) - Q = 0 F; (b) – Q = 1 F; (c) – Q = 2 F.

The solution after the electrolysis, the aqueous solution of separated particles and the solution above the precipitate were investigated using DLS technique (Figure 9). In the first case, the average size of the NP is 44 nm (PdI = 0.548 ± 0.083). After purification, the average size becomes 18 nm (PdI = 0.292 ± 0.023). The zeta potential of these particles is 66.8 ± 0.6 mV. The hydrodynamic diameters of the NP in the solution above the sediment are 1.4 nm (PdI = 0.476 ± 0.026), perhaps the data can correspond to micelles of CTAC.

Studies by various microscopic methods showed that very small NP are formed. As it is seen from the SEM images (Figure 10a), the particles are combined into larger aggregates by adhesion of organic shells. The energy-dispersive spectrum (Figure 10b) demonstrates that the NP are composed mainly of metallic palladium, as well as of an organic ingredient (CTAC stabilizer).

TEM and STEM (Figure 11) images show that the metal nanoparticles are generally spherical in shape and their size is 5 ± 3 nm. A histogram of particle size distribution is shown in Figure 12.

According to the analysis by XPRD, the diffraction pattern of the sample studied is a result of combined scattering from both the palladium crystalline phase and several other crystalline components present in the precipitate (Figure 13). The presence of palladium is confirmed by a search of experimental X-ray diffraction patterns in

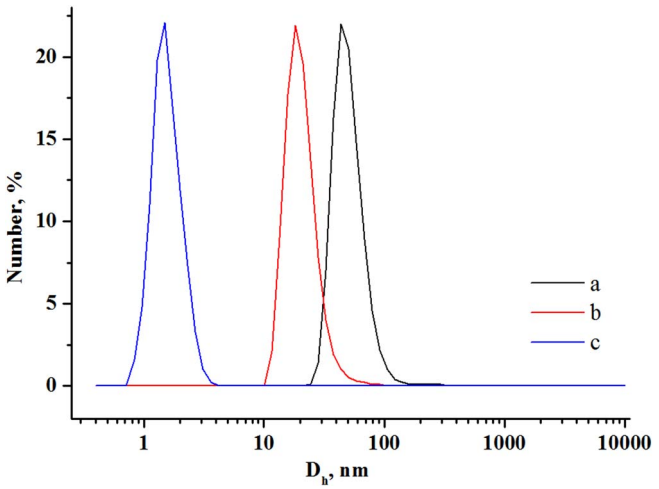

Figure 9. Size distribution diagram of PdNp stabilized with CTAC in water: (a) in electrolyzate, (b) after separation, (c) in the solution above the precipitate.

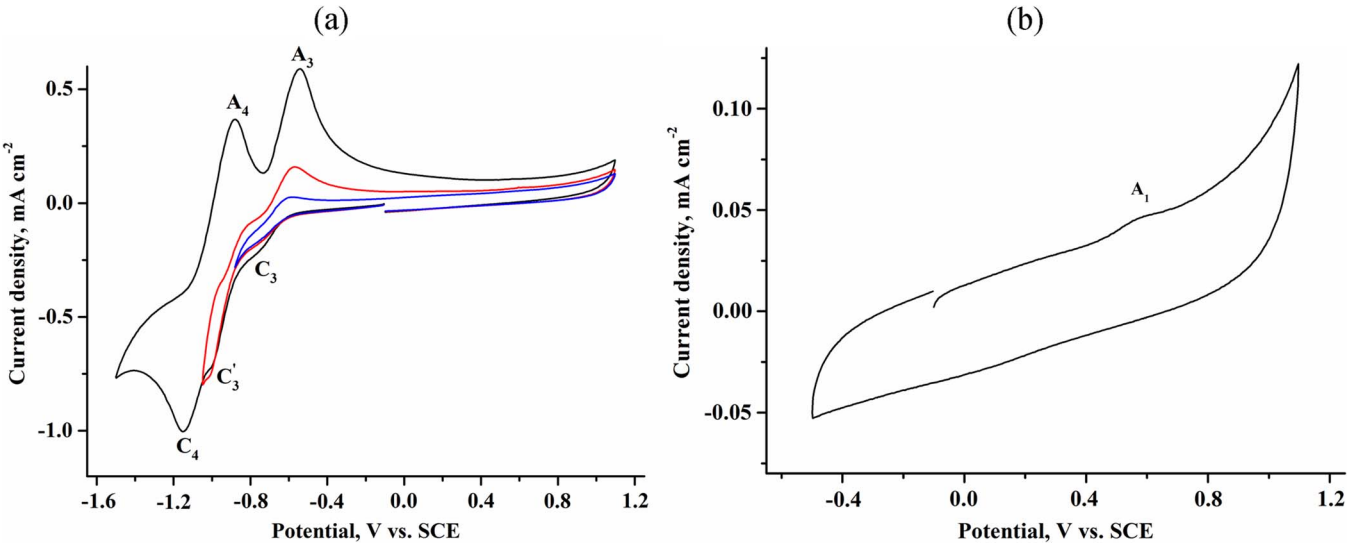

Figure 8. CV curves of the $[PdCl_4]^{2-}$ (1.5 mM) – MV^{2+} (2 mM) system in water /0.02 M CTAC medium after electrolysis at E = −0.90 V (Q = 2 F/mol $[PdCl_4]^{2-}$) recorded (a) at once and (b) after exposure of the electrode in the solution for 3 min without stirring and without applying potential. $E_{start.}$ = −0.10 V. ν = 100 mV/s.

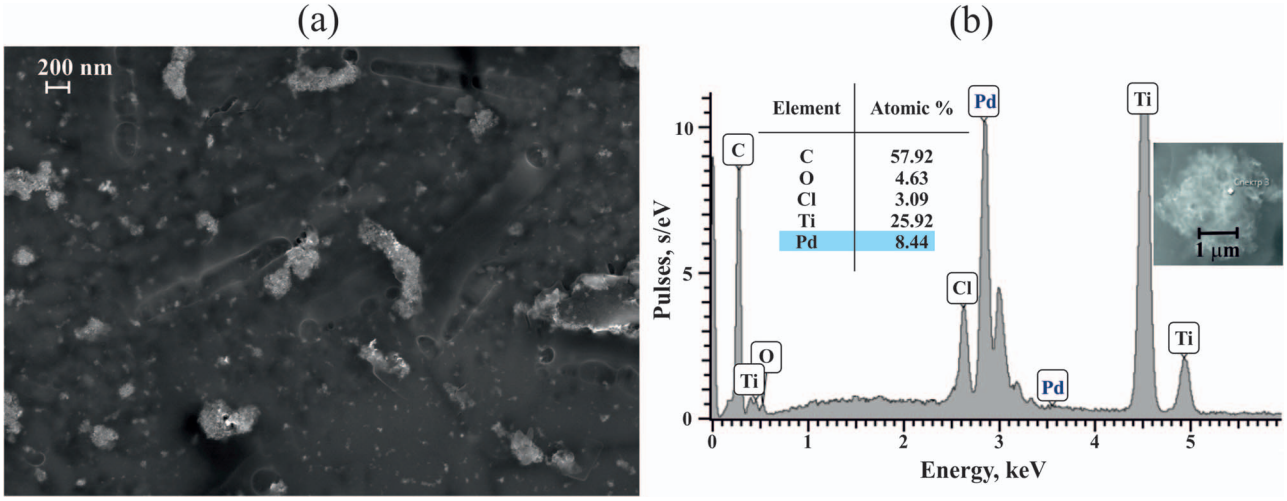

Figure 10. (a) SEM image and (b) energy-dispersion spectrum of PdNp stabilized with CTAC on a titanium support. On the insert (b) the cross shows the section from which the energy-dispersion spectrum is recorded.

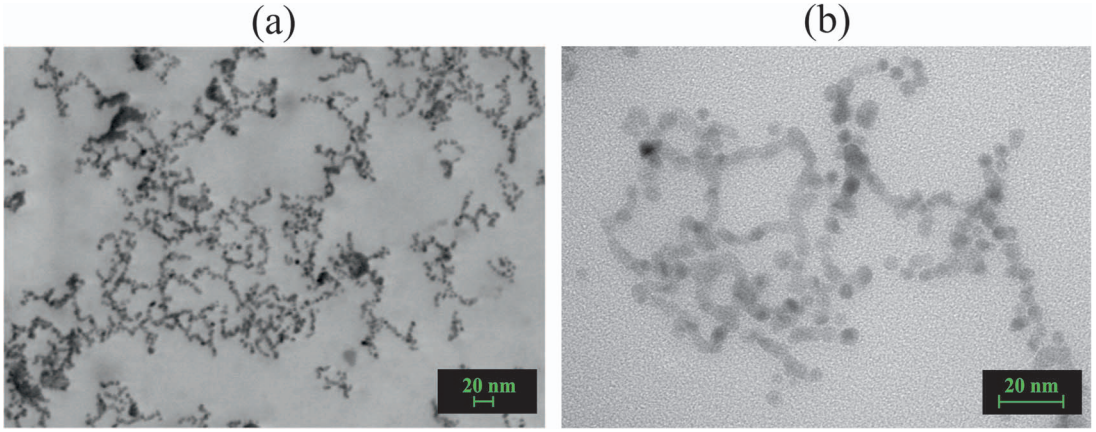

Figure 11. (a) STEM and (b) HRTEM images of PdNp stabilized with CTAC.

PDF-2 powder diffractometry database. The search led to a suitable compound (the cubic form of palladium: *Palladium, syn, code No. 00-005-0681*). The positions of the diffraction peaks of the latter are shown in Figure 13.

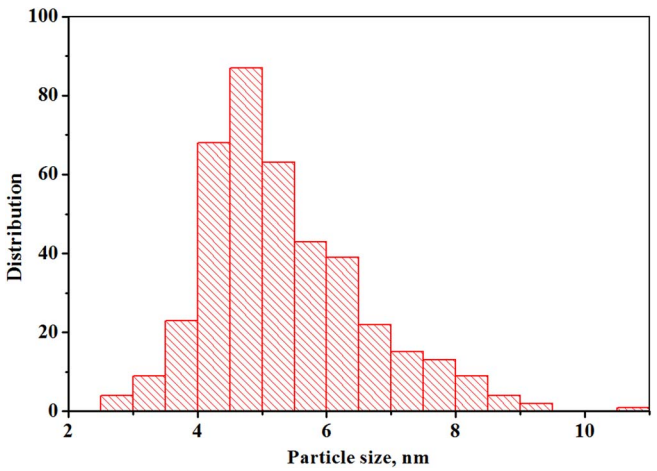

Figure 12. Histogram of particle size distribution measured from HRTEM image.

The diffuse nature of the majority of palladium diffraction peaks indicates the small linear dimensions of the palladium crystallites, i.e. its nanostructuring. In addition, the sample contains a certain amount of other crystalline substances.

Taking into account the additive character of diffraction patterns of polycrystalline substances, in the case of a mechanical mixture of two or more components, interference peaks corresponding to all its components (with their quantities in the mixture taken into account) should be observed in the resulting diffraction pattern. It should be noted that the sensitivity of the XPRD method in the detection of a crystalline phase for organic compounds is in the range of 0.1% or higher, while the amount of crystalline components in the sample is much larger. Assuming that methylviologen and CTAC can be these crystalline components, XRPD experiments with these compounds were carried out (Figures 13b,13c). The results of comparison between the diffraction patterns support the presence of these substances as impurities in the precipitate being studied. Small differences in the shape and intensity of a number of diffraction peaks are probably associated with some difference in the dispersion of the powders and minor texturing of the samples that occurs during their alignment on the surface of the holder. The presence of additional peaks may also be due to the presence of trace amounts of other crystalline components that have not been analyzed. Full-profile analysis of experimental diffraction data and refinement of the results obtained by the Rietveld method were performed using TOPAS software package.[50] The crystalline palladium was analyzed as a separate phase, and the remaining crystalline components of the precipitate were included in the

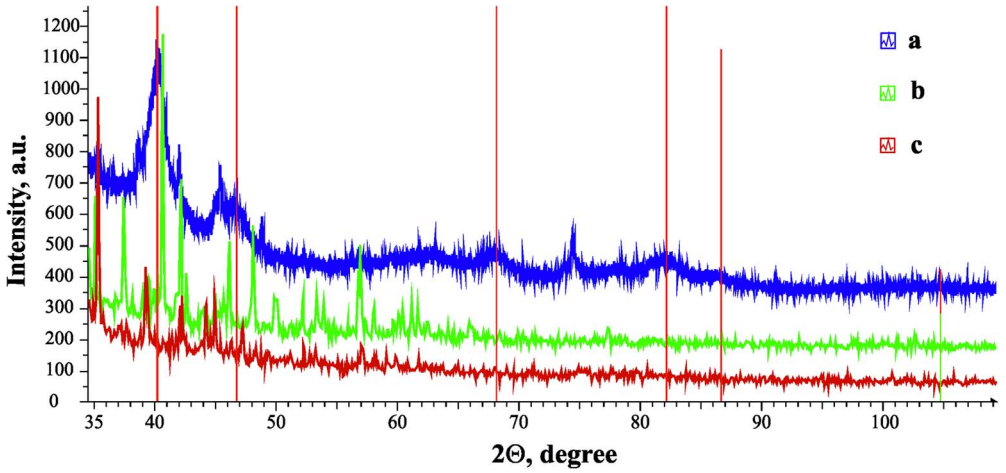

Figure 13. (a) The experimental diffraction patterns of examined sample, (b) CTAC and (c) $MVCl_2$. For clarity, the curves are shifted relative to each other along the intensity axis. Red vertical lines show the positions of the interference peaks corresponding to crystalline palladium, syn., code no. 00-005-068.

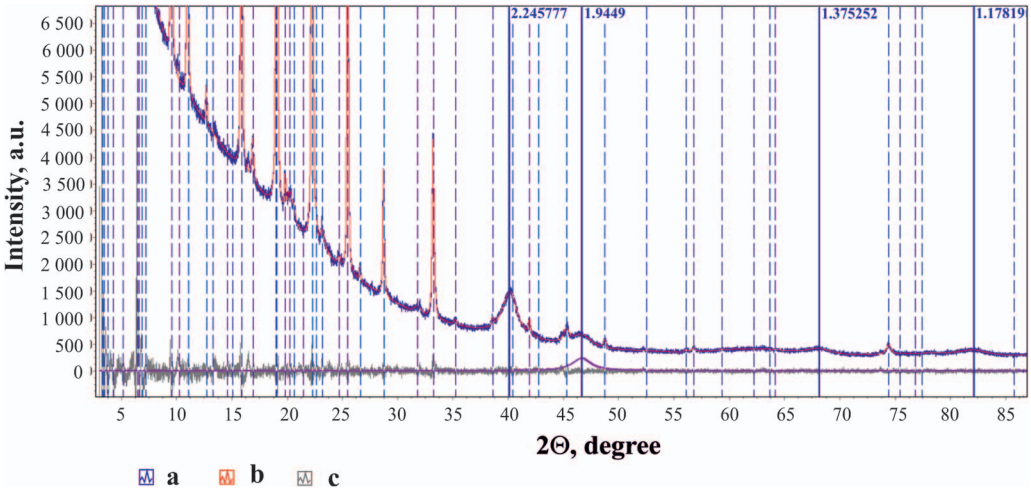

Figure 14. (a) The experimental diffraction patterns of the precipitate sample, (b) the theoretically calculated summary curve and (c) the residual difference curve. The continuous vertical lines show the positions of the interference peaks corresponding to crystalline palladium, syn., code no. 00-005-068. The dashed vertical lines show the positions of the peaks of the other crystalline phases.

second phase and were not analyzed in detail (the results of refinement are presented in Figure 14). The correctness of the comparison of model (theoretical) and experimental curves was provided by minimization of R_{wp} convergence parameter. An additional visual criterion for convergence of the results is provided by the difference curve. Its deviation from zero would mean incomplete identification of the composition.

The calculated palladium crystallite sizes obtained from analysis of the observed diffraction peaks of palladium are shown in Table I. The resulting average effective crystallite size is 4.66 nm.

Table I. The results of calculations of palladium crystallite size.

Miller indexes of reflections	d, Å	intensity, a.u.	Crystallite size, nm
111	2.248(3)	161	5.4(6)
200	1.945(2)	81	4.7(5)
220	1.3755(8)	113	4.2(5)
311	1.1734(7)	130	4.3(7)
222	1.125(1)	55	4.7(2)

Summary

In development of the method for mediated electrosynthesis of MNP, the possibility of methylviologen mediated electrosynthesis of ultrasmall PdNP (5 ± 3 nm) in an aqueous medium using CTAC as a stabilizer was demonstrated in this study. The formation of poorly soluble $([PdCl_4]^{2-} \cdot 2CTA^+)_n$ aggregates leads to slow direct reduction of $[PdCl_4]^{2-}$ on the electrode and deposition of the generated metal on it. However, in the case of mediated reduction at potentials of the $MV^{2+}/MV^{\bullet+}$ redox couple, the process is rapid, the metal is not deposited on the cathode, and on passing of $Q = 2$ F quantitative conversion from $[PdCl_4]^{2-}$ to nanoparticles of $Pd@CTA^+$ (the hydrodynamic diameter is 18 nm, the zeta-potential is 66.8 mV) occurs in the solution bulk. Separated nanoparticles of Pd@CTAC are combined into larger aggregates of different shapes due to coalescence of the organic shells. The metal core of the particles has the shape of imperfect sphere the average size of which is 5 ± 3 nm. The XPRD method shows that the resulting NP contain palladium crystallites with an average size of 4.66 nm.

Acknowledgment

The authors acknowledge the financial support from RFBR (grant no. 14-03-00405 and no. 16-33-00420 мол_а).

References

1. A. D. Pomogailo, A. S. Rozenberg, and I. E. Uflyand, *Metal nanoparticles in polymers*, 672 p., Khimia, Moscow (2000).
2. V. I. Roldughin, *Russ. Chem. Rev.*, **69**, 821 (2000).
3. M.-C. Daniel and D. Astruc, *Chem. Rev.*, **104**, 293 (2004).
4. I. P. Suzdalev, *Nanotechnology: physicochemistry of nanoclusters, nanostructures and nanomaterials*, 589 p., Librokom, Moscow (2009).
5. V. V. Volkov, T. A. Kravchenko, and V. I. Roldughin, *Russ. Chem. Rev.*, **82**, 465 (2013).
6. L. A. Dykman, V. A. Bogatyrev, S. Yu. Shchyogolev, and N. G. Khlebtsov, *Gold nanoparticles. Synthesis, properties and biomedical applications*, 319 p., Nauka, Moscow (2008).
7. B. I. Kharisov, O. V. Kharissova, and U. Ortiz-Mendez, *Handbook of less-common nanostructures*, 828 p., CRC Press, Taylor & Francis Group, Boca Raton (2012).
8. O. A. Petrii, *Russ. Chem. Rev.*, **84**, 159 (2015)
9. L. Rodrigues-Sanchez, M. L. Blanko, and M. A. Lopez-Quintela, *J. Phys. Chem.*, **104**, 9683 (2000).
10. B. Yin, H. Ma, S. Wang, and S. Chen, *J. Phys. Chem. B*, **107**, 8898 (2003).
11. V. Saez and T. J. Mason, *Molecules*, **14**, 4284 (2009).
12. J. Zhu, S. Liu, O. Palchik, Y. Koltypin, and A. Gedanken, *Langmuir*, **16**, 6396 (2000).
13. J. Reisse, T. Caulier, C. Deckerkheer, O. Fabre, J. Vandercammen, J. L. Delplancke, and R. Winand, *Ultrason. Sonochem.*, **3**, 147 (1996).
14. M. T. Reetz and W. Helbig, *J. Am. Chem. Soc.*, **116**, 7401 (1994).
15. J. A. Becker, R. Schäfer, R. Festag, W. Ruland, J. H. Wendorff, J. Pebler, S. A. Quaiser, W. Helbig, and M. T. Reetz, *J. Chem. Phys.*, **103**, 2520 (1995).
16. M. T. Reetz, S. A. Quaiser, and C. Merk, *Chem. Ber.*, **129**, 741 (1996).
17. M. T. Reetz, W. Helbig, S. A. Quaiser, U. Stimming, N. Breuer, and R. Vogel, *Science*, **267**, 367 (1995).
18. M. T. Reetz, M. Winter, R. Breinbauer, T. Thurn-Albrecht, and W. Vogel, *Chem. Eur. J.*, **7**, 1084 (2001).
19. M. T. Reetz, W. Helbig, and S. A. Quaiser, *Chem. Mater.*, **7**, 2227 (1995).
20. Y. Li, Q. Qiang, X. Zheng, and Z. Wang, *Electrochem. Commun.*, **58**, 41 (2015).
21. N. Vilar-Vidal, M. C. Blanco, M. A. López-Quintela, J. Rivas, and C. Serra, *J. Phys. Chem. C*, **114**, 15924 (2010).
22. Yu-Y. Yu, S.-S. Chang, Ch.-L. Lee, and C. R. Ch. Wang, *J. Phys. Chem. B*, **101**, 6661 (1997).
23. M. B. Mohamed, Z. L. Wang, and M. A. El-Sayed, *J. Phys. Chem. A*, **103**, 10255 (1999).
24. V. V. Yanilkin, G. R. Nasybullina, A. Yu. Ziganshina, I. R. Nizamiev, M. K. Kadirov, D. E. Korshin, and A. I. Konovalov, *Mendeleev Commun.*, **24**, 108 (2014).
25. V. V. Yanilkin, G. R. Nasybullina, E. D. Sultanova, A. Yu. Ziganshina, and A. I. Konovalov, *Russ. Chem. Bull., Int. Ed.*, **63**, 1409 (2014).
26. V. V. Yanilkin, N. V. Nastapova, G. R. Nasretdinova, R. K. Mukhitova, A. Yu. Ziganshina, I. R. Nizameev, and M. K. Kadirov, *Russ. J. Electrochem.*, **51**, 951 (2015).
27. S. Fedorenko, M. Jilkin, N. Nastapova, V. Yanilkin, O. Bochkova, V. Buriliov, I. Nizameev, G. Nasretdinova, M. Kadirov, A. Mustafina, and Y. Budnikova, *Colloids Surf., A*, **486**, 185 (2015).
28. V. V. Yanilkin, N. V. Nastapova, E. D. Sultanova, G. R. Nasretdinova, R. K. Mukhitova, A. Y. Ziganshina, I. R. Nizameev, and M. K. Kadirov, *Izv. AN, ser chim.*, **1**, 125 (2016).
29. G. R. Nasretdinova, R. R. Fazleeva, R. K. Mukhitova, I. R. Nizameev, M. K. Kadirov, A. Yu. Ziganshina, and V. V. Yanilkin, *Electrochem. Commun.*, **50**, 69 (2015).
30. G. R. Nasretdinova, R. R. Fazleeva, R. K. Mukhitova, I. R. Nizameev, M. K. Kadirov, A. Yu. Ziganshina, and V. V. Yanilkin, *Russ. J. Electrochem.*, **51**, 1029 (2015).
31. V. V. Yanilkin, N. V. Nastapova, G. R. Nasretdinova, R. R. Fazleeva, A. V. Toropchina, and Yu. N. Osin, *Electrochem. Commun.*, **59**, 60 (2015).
32. G. R. Nasretdinova, R. R. Fazleeva, Y. N. Osin, A. T. Gubaidullin, and V. V. Yanilkin, *Russ. J. Electrochem*, in press (2016).
33. V. V. Yanilkin, G. R. Nasretdinova, Yu. N. Osin, and V. V. Salnikov, *Electrochim. Acta*, **168**, 82 (2015).
34. V. V. Yanilkin, N. V. Nastapova, G. R. Nasretdinova, S. V. Fedorenko, M. E. Jilkin, A. R. Mustafina, A. T. Gubaidullin, and Y. N. Osin, *RSC Advances*, **6**, 1851 (2016).
35. Y. Xia, X. Xia, and H. C. Peng, *J. Am. Chem. Soc.*, **137**, 7947 (2015).
36. J. Li, P. Zhou, F. Li, J. Ma, Y. Liu, X. Zhang, H. Huo, J. Jin, and J. Ma, *J. Power Sources*, **302**, 343 (2016).
37. L. Graham, G. Collins, J. D. Holmes, and R. D. Tilley, *Nanoscale*, **8**, 2867 (2016).
38. Y.-H. Chen, H.-H. Hung, and M. H. Huang, *J. Am. Chem. Soc.*, **131**, 9114 (2009).
39. F. Wang, C. Li, L.-D. Sun, C.-H. Xu, J. Wang, J. C. Yu, and C.-H. Yan, *Angew. Chem., Int. Ed.*, **51**, 4872 (2012).
40. J. P. Wolfe, R. A. Singer, B. H. Yang, and S. L. Buchwald, *J. Am. Chem. Soc.*, **121**, 9950 (1999).
41. M. Pérez-Lorenzo, *J. Phys. Chem. Lett.*, **3**, 167 (2012).
42. T. V. Magdesieva, O. M. Nikitin, O. A. Levitsky, V. A. Zinovyeva, I. Bezverkhyy, E. V. Zolotukhina, and M. A. Vorotyntsev, *J. Mol. Cat. A: Chemical*, **353–354**, 50 (2012).
43. A. Bej, K. Ghosh, A. Sarkar, and D. W. Knight, *RSC Adv.*, **6**, 11446 (2016).
44. G. Zhang, H. Zhou, J. Hu, M. Liu, and Y. Kuang, *Green Chem.*, **11**, 1428 (2009).
45. A. Kamal, V. Srinivasulu, B. N. Seshadri, N. Markandeya, A. Alarifi, and N. Shankaraiah, *Green Chem.*, **14**, 2513 (2012).
46. T. V. Magdesieva, O. M. Nikitin, E. V. Zolotukhina, V. A. Zinovyeva, and M. A. Vorotyntsev, *Mendeleev commun.*, **22**, 305 (2012).
47. D. B. Pacardo, M. Sethi, S. E. Jones, R. R. Naik, and M. R. Knecht, *ACS Nano*, **3**, 1288 (2009).
48. J. C. Garcia-Martinez, R. Lezutekong, and R. M. Crooks, *J. Am. Chem. Soc.*, **127**, 5097 (2005).
49. DIFFRAC Plus Evaluation package EVA, Version 11, User's Manual, 258 p., Bruker AXS, Karlsruhe, Germany (2005).
50. TOPAS V3: General profile and structure analysis software for powder diffraction data. Technical Reference, 117 p., Bruker AXS, Karlsruhe, Germany (2005).
51. N. V. Korovin, *Corrosion and electrochemical properties of palladium*, 239 p., Metallurgiya, Moscow (1976).